Modeling contact deformation of bare and coated rough metal bodies

Civiero, R.; Perez-Rafols, F.; Nicola, L.

DOI
10.1016/j.mechmat.2023.104583

Publication date
2023

Document Version
Final published version

Published in
Mechanics of Materials

Mechanics of Materials 179 (2023) 104583

Contents lists available at ScienceDirect

Mechanics of Materials

journal homepage: www.elsevier.com/locate/mecmat

Research paper

Modeling contact deformation of bare and coated rough metal bodies

R. Civiero [a], F. Perez-Rafols [a,b], L. Nicola [a,c,*]

[a] Department of Industrial Engineering, University of Padua, Via Venezia 1, 35131, Padua, Italy
[b] Serra Hunter Fellow at the Department of Mining, Industrial and ICT Engineering, Universitat Politécnica de Catalunya, Barcelona, Spain
[c] Department of Materials Science and Engineering, Delft University of Technology, 2628CD Delft, The Netherlands

ARTICLE INFO

Keywords:
Dislocation dynamics
Contact mechanics
Self-affine surfaces
Strain hardening

ABSTRACT

The effect of the presence of a passivation layer on a metal rough surface during contact loading is investigated by means of dislocation dynamics simulations. The metal body is modeled as an FCC single crystal with a self-affine rough surface that is either bare, or covered by a thin coating, impenetrable to dislocations. This analysis permits to isolate the effect of surface roughening driven by dislocation motion: when the surface is bare the dislocations can glide out, leaving crystallographic steps at the surface that modify the local roughness; when the surface is passivated, dislocations are stopped by the interface.

1. Introduction

It has been observed that metal surfaces have self-affine roughness with a Hurst exponent typically ranging between 0.7 and 0.9 (Plouraboué and Boehm, 1999; Bouchaud, 1997). From the early 50's, various models have been proposed to predict the contact response of solids with rough surfaces, mostly focusing on their elastic behavior. The most widely applied are the so-called asperity models, based on the pioneering work of Greenwood and Williamson (1966), who relied on Hertz theory and treated the rough surface as a collection of spherical asperities distributed along the height of the surface. Asperity models, lately extended to include elastic interactions (Ciavarella et al., 2008), and coalescence of the contact areas (Afferrante et al., 2012), are rather accurate at small contact fractions. For comprehensive reviews on the topic the reader is referred to the work by Carbone and Bottiglione (2008) and Paggi and Ciavarella (2010). A very elegant and innovative approach to contact mechanics was proposed at the beginning of the century by Persson (2001b) who provided the pressure distribution as a function of the magnification of the surface topography. Contrary to asperity models, Persson's theory is more accurate at large contact fractions and can be applied up to full contact, where it is exact. In the past years, contact problems between rough surfaces have been addressed extensively by means of computer simulations, mostly by means of boundary elements methods (Almqvist et al., 2007; Tiwari et al., 2020; Ilincic et al., 2009). Provided that the rough surface is discretized sufficiently fine as to account for the short wavelengths in the roughness, various numerical techniques can provide a converged solution to the contact problem and track the variation of the true contact area with increasing load, in good agreement with dedicated experiments (Müser et al., 2017).

All elastic models predict at small loads a true contact area much smaller than the nominal contact area, and a contact pressure significantly larger than the nominal contact pressure. It is thus expected that already at moderate applied loads, the yield stress of metallic materials is exceeded, at least under the nano- and micro-scale contact areas (Yamada et al., 1978; Woo and Thomas, 1980). Therefore, when metals are pressed into light contact, the response is believed to deviate significantly from linear elasticity, as the asperities are squeezed plastically. Unfortunately a measure of true contact area and local contact pressure cannot be obtained in non-transparent materials, and accurate experimental data is lacking.

The effect of plasticity on the contact response of rough surfaces with Gaussian height distribution was first considered by Pullen et al. (1972) who noticed that rough surfaces never fully flatten, independently of how large is the applied load. Although this observation is an indication of strain hardening, they describe plasticity without considering any hardening. They based their model on the evidence that plastic deformation conserves volume and assumed that the material displaced during contact would reappear as a homogeneous raise of the valleys. Chang et al. (1987) provided an asperity model that includes plasticity at a given interference with an expression of the contact area that at small loads converges to the elastic Greenwood–Williamson solution and at large loads to the plastic Pullen–Williamson's. Also Persson's model has been modified to describe bodies that deform in an elastic-perfectly plastic manner (Persson, 2001a).

A more realistic description of plasticity, including strain hardening, was considered by Pei et al. (2005), who conducted a careful finite element analysis of the contact response of rough metal bodies. One

* Corresponding author at: Department of Materials Science and Engineering, Delft University of Technology, 2628CD Delft, The Netherlands.
E-mail address: lucia.nicola@unipd.it (L. Nicola).

https://doi.org/10.1016/j.mechmat.2023.104583
Received 26 September 2022; Received in revised form 25 January 2023; Accepted 31 January 2023
Available online 4 February 2023

of their main findings is that the real contact area varies linearly with load in the plastic regime, albeit with a different slope than in the elastic regime, for various values of the yield strength. Values provided by models based on continuum plasticity find mean contact pressures of about five to six times the yield strength of the material (Gao and Bower, 2006).

Numerical models based on discrete dislocation plasticity display strain hardening as an emergent behavior, caused mostly by a limited mobility of the dislocations owing to their interaction with other dislocations or their pinning at precipitates or interfaces. Through dislocation dynamics simulations, Venugopalan and Nicola (2019) have also found a linear relationship between load and area. Moreover, they have shown that classical plasticity overestimates the amount of plastic deformation in rough contacts: at small contact fractions the discrete nature of dislocation sources, and thus their limited availability in contact regions, favors a later onset of plasticity and a more pronounced strain hardening than observed in classical plasticity. The contact pressure would rise closer to the contact pressure calculated elastically than to that calculated through classical plasticity. Most importantly in the framework of this work, a pronounced roughening of the surface was found upon contact deformation in simulations where a metal flat surface was indented by a rigid rough body. The roughening was caused by dislocations gliding out of the free surface and leaving there crystallographic steps.

Such type of roughening could not be captured by classical plasticity, but is a signature of metal plasticity observed for instance in experiments of scratching of metal surfaces (Brinckmann and Dehm, 2015; Xia et al., 2020). The question we would like to address in this work is to which extent dislocation roughening might affect the evolution of contact deformation and pressure.

In the simulations performed by Venugopalan and Nicola (2019) and by Irani and Nicola (2019) the metal surface was taken to be flat and bare, and therefore the roughening due to the exit of dislocations appeared very pronounced. Real metallic surfaces are mostly covered by coatings or native oxides, which act as partial barriers to dislocations. In the presence of such a barrier the roughening due to dislocations exiting the surface is likely to be significantly reduced if not fully hampered. The aim of this work is to investigate to which extent the presence of an impenetrable coating affects plastic deformation of a metal rough crystal. More specifically, by contrasting the contact behavior of a bare and a coated crystal with the same roughness, we aim at isolating and estimating the effect of surface roughening driven by dislocation plasticity. This is of interest because the local change in surface topography might lead to a change in the contact area and consequently on all related properties, as contact pressure, friction, adhesion or leakage.

2. Formulation of the problem and methodology

Coated and bare flat metallic crystals are indented by a rigid body with a self-affine rough surface. The simulations are performed on a two-dimensional unit cell under plane strain conditions. The crystals are first indented quasi-statically; thereafter, the punch is gradually retracted with the same slow rate used during indentation. The contact surfaces are prescribed to be frictionless at the contact points, and traction-free elsewhere; the bottom of the cell is fixed.

The solution to this boundary value problem is obtained by means of the Green's Function Dislocation Dynamics method, described in detail in Venugopalan et al. (2017). Following Van der Giessen and Needleman (1995), the displacement, strains and stresses in the dislocated body are obtained, at every incremental displacement of the indenter, as the superposition of two linear elastic fields: the analytical fields of the dislocations in an infinite elastic medium, and their image fields. The image fields are calculated using a Green's function boundary element method that finds the deformed surface by means of damped dynamics (Campañá and Müser, 2007). The Green's function method, known as Green's function molecular dynamics, is based on the small-slope and on the small-strains assumptions, and therefore finds the image fields of the dislocations as if they were mirrored on the original flat surface, despite the surface roughens. The schematic representation of the solution procedure is shown in Fig. 1.

At the beginning of the simulation the body is dislocations free, but contains a given density of nucleation point sources, resembling Frank-Read sources in two dimensions. These sources are equally distributed on the three sets of parallel slip planes on which the dislocations can nucleate and glide. The configuration we use to represent the crystal structure follows the indication provided by Rice (1987) on how the deformation of an FCC crystal can be idealized in a 2D representation that uses plane strain conditions (see Fig. 2 for a sketch). The plane of deformation is the (110) plane. In this orientation, dislocation loops can form that are extended in the out-of-plane direction and that in the plane strain limit are straight and of edge character. Equal slip along the two face diagonals of the $(\bar{1}11)$ and $(1\bar{1}1)$ slip planes is consistent with the [110] direction being perpendicular to the plane of deformation. Thus, slip on the $(\bar{1}11)$ plane (red in Fig. 2) effectively occurs in the $[1\bar{1}2]$ direction, while similarly on the $(1\bar{1}1)$ plane (green) slip effectively occurs in the $[\bar{1}12]$ direction. Another deformation possibility is slip in the [110] direction on the (111) slip plane (blue). This does not correspond to a dislocation in the (110) plane (which therefore is dashed in Fig. 2), but since symmetry demands equal slip on the $(\bar{1}\bar{1}1)$ plane, the composition of these is equivalent to slip on the (001) plane. On the (110) plane the slip directions are therefore inclined at ±54.7° and 0° with the $[\bar{1}10]$ direction, which we identify with the x_1 axis. In this work, we have approximated the ±54.7° with ±60°, and rotated the crystal by ±15° to avoid having planes perfectly orthogonal to the loading direction, which is rather unlikely to happen in actual experiments.

The Frank Read sources generate a dislocation dipole, which is the 2D representation of a dislocation loop, once the resolved shear stress they experience overcomes their critical strength τ_{nuc}, for a critical time t_{nuc}. After nucleation, the dislocations glide on the slip planes with a velocity proportional to the Peach–Koehler force acting on the

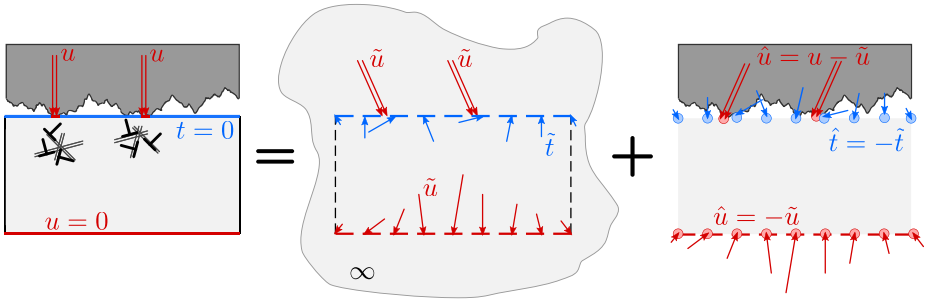

Fig. 1. The solution of the indentation boundary value problem, represented schematically on the left-hand side of the 'equation', is obtained by superposition of the fields of the dislocations in an infinite solid, and their image fields, shown on the right-hand side. The crystal in the figure is stretched in vertical direction to visualize the roughness. The edge dislocations are represented by black ⊤-symbols.

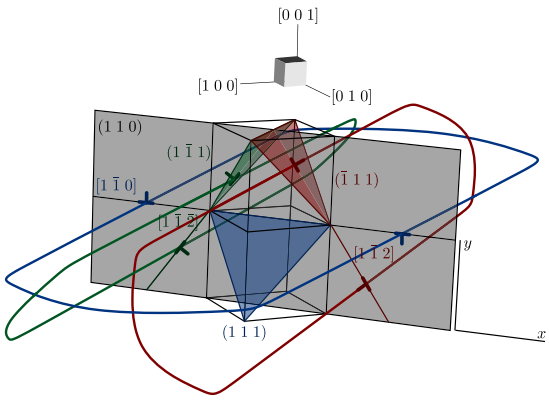

Fig. 2. Two-dimensional representation of an FCC crystal on the (1 1 0) plane. The slip traces form 54.75° angles with respect to the x axis. The colored triangles represent the (1 1 1) slip planes, the three colored loops represent the three-dimensional dislocation loops, gliding on the [1 1 2] directions, while the 2D dislocations are represented with the ⊤ symbol.

dislocation and limited by the drag coefficient. When two dislocations of opposite sign approach each other very closely ($6b$, where b is the Burgers vector length), they are removed from the simulation to mimic annihilation. If the dislocations are instead equally signed, they are merged, if closer than $2b$, into a superdislocation with combined Burgers vector. Merging of the Burgers vectors occurs only sporadically in the simulations, in about 0.1% of the pile-ups and was tested to have negligible impact on the results. It has, however, the positive effect of speeding up the calculation significantly, as the high speed vibration of a dislocation in a closely spaced pile-up does require a very small time step, which needs to be imposed to the whole system.

Similarly to dislocations sources, dislocation point obstacles are randomly distributed inside the body on the slip planes. Once dislocations reach them, they are pinned, and released only once the resolved shear stress on them overcomes the critical strength of the obstacles τ_{obs}, or if the dislocation reverts its motion. When the substrate is bare, dislocations can exit the free surface, leaving crystallographic steps; when the substrate is coated, dislocations are blocked at the interface. To model the presence of a coating impenetrable to dislocations, impenetrable obstacles are placed at the interface between coating and metal crystal. This coating is assumed to have identical elastic constants as the substrate, to have uniform thickness, and to be fully adherent to the metal (Chen and Etsion, 2019). In this way the impenetrable interface to dislocations is the only difference between the bare and coated substrate, and its effect can be clearly evaluated.

2.1. Choice of parameters

The surface is indented with a constant rate $\dot{u} = 2 \cdot 10^4$ μm/s until a depth $u = 75$ nm. A convergence analysis was performed to find the speed at which the simulation can be considered quasi-static, i.e., the results are independent of a further reduction of the indentation rate.

The substrate is taken to be made of aluminum, with elastic modulus $E = 70$ GPa, Poisson's ratio $\nu = 0.33$, and Burgers vector length $b = 2.86$ Å. The height of the crystal is chosen to be $h = 20$ μm, which is significantly larger than the thickness of the passivation layer, which is $h_{\text{p}} = 0.1$ μm. The periodic unit cell is taken to have width $w = 20$ μm.

The parameters selected to describe plasticity are taken similar to those in Venugopalan et al. (2017): The density of sources and obstacles is taken to be $\varrho_{\text{nuc}} = 40$ μm^{-2} and $\varrho_{\text{obs}} = 40$ μm^{-2} respectively. The nucleation time is $t_{\text{nuc}} = 10$ ns. The nucleation source strength has a Gaussian distribution around a mean value of $\tau_{\text{nuc}} = 50$ MPa, with a standard deviation of 10 MPa. The obstacle critical strength is set to $\tau_{\text{obs}} = 150$ MPa.

To generate the self-affine surface topography of the body, the power spectral density method is used (Hu and Tonder, 1992). The Hurst exponent is taken to be 0.8, a typical value for metallic surfaces (Plouraboué and Boehm, 1999). The long-wavelength cutoff is $\lambda_l = 10$ μm, while the fractal discretization is selected to be $\varepsilon_f = \lambda_s/\lambda_l = 512^{-1}$. λ_s is the short-wavelength cut-off, which is therefore equal to 19.5 nm.

While metallic surfaces have root-mean-square height ranging typically between 0.3 μm to 2.5 μm (Plouraboué and Boehm, 1999), we selected for this study $h_{\text{rms}} = 0.075$ μm, lower than the typical range to achieve a seizable contact area while satisfying the small strain assumption. Only the top and bottom surfaces of the body are discretized by means of 2^{14} nodes, corresponding to a nodal spacing of 1.22 nm. The fine spacing is necessary to resolve accurately the roughness and the variation in contact area. The position Verlet algorithm is used to compute through damped dynamics the displacement of the nodes that are not directly coupled to a force. The dimensionless time-step selected for the damped dynamics is $\tau = 0.25$. The damping factor selected is:

$$\eta \propto \frac{1}{\tau}\sqrt{\frac{2(1+\nu)}{E}\frac{L_{\text{y}} N_{\text{nodes}}}{L_{\text{x}}}} \tag{1}$$

3. Results and discussion

3.1. Contact pressure, area, and dislocation activity

Two metal crystals, one bare, the other coated by an impenetrable, 100 nm thick layer, are slowly indented by the same rough rigid punch to a depth of 75 nm. The punch is then retracted with the same slow speed used during indentation. The change in nominal pressure P_{n}, normalized on the dislocation source strength, τ_{nuc}, with the applied indentation depth is presented in Fig. 3(a) for both the bare and coated metal crystals. The corresponding variation in contact fraction is presented in Fig. 3(b). After a first predominantly elastic response, where only a few dislocations are nucleated and the two curves overlap, plasticity becomes evident in the bare film and the curves start to diverge at around $u = 13$ nm. The coated layer displays a harder response, owing to the barrier to dislocations posed by the interface. Both curves present a rather pronounced increase in slope when a new contact patch is formed. The coated layer is subject to a larger pressure at final indentation depth than the bare layer, and presents a smaller remnant plastic strain after unloading. Therefore, as expected, the evidence points to a larger plastic activity in the bare crystal.

To gain understanding of the different dislocation activity in the two crystals, Fig. 4 presents the distribution of the dislocations together with the distribution of the normal stress σ_{yy}, normalized by the average nucleation strength, τ_{nuc}, at $u = 40$ nm (top figures), at $u = 75$ nm (middle figures) and after retraction of the indenter (bottom figures). The bare crystal is on the left-hand side and the coated crystal on the right-hand side. In the two upper figures, corresponding to an indentation depth of $u = 40$ nm, the indenter has made contact with the bare and coated crystals mostly through three asperities. The first two asperities that entered into contact are at the center of the unit cell, very close to each other, and the third one, which entered into contact later is on the right-hand side of the cell. The dislocations that have nucleated underneath the contacts due to the stress imposed by the asperities, are concentrated on a few slip planes and form shear bands that extend rather deep in the crystal. In particular, the ones on the planes forming 15° with the indentation direction reach a depth considerably larger than the contact size. These long and localized shear bands are a characteristic feature of crystal plasticity that is an emergent behavior in dislocation dynamics simulation, and cannot be predicted by classical plasticity. At maximum indentation depth (Fig. 4 (c) and (d)) more asperities make contact with the crystal and the dislocation density increases significantly, especially in a top band of the crystal of about five micrometers thickness. When the dislocation

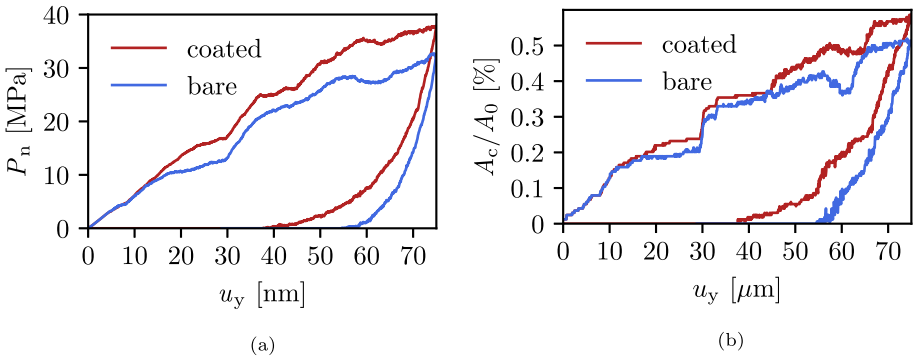

Fig. 3. Variation of nominal contact pressure 3(a) and contact fraction 3(b) for the indentation of a bare and coated crystals to a depth of 75 nm, and subsequent retraction of the indenter.

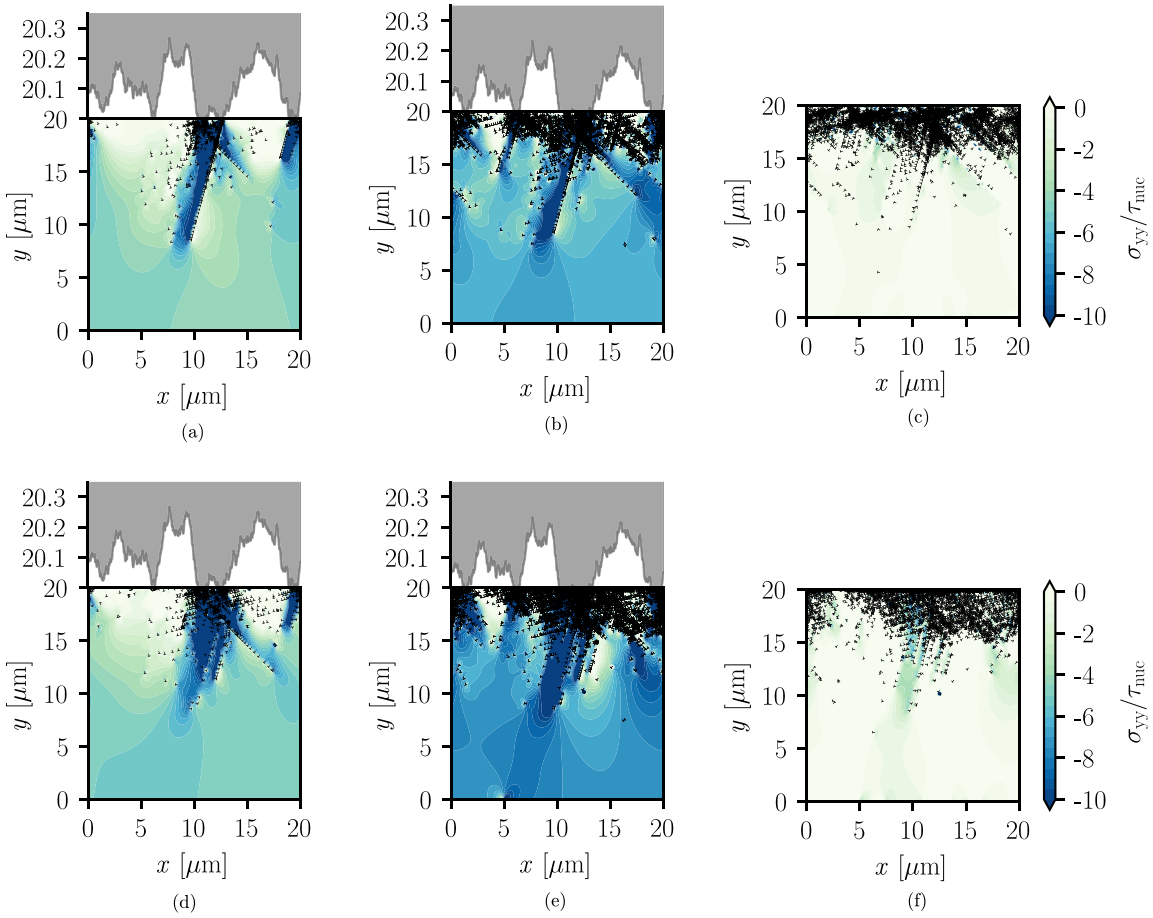

Fig. 4. Distribution of the dislocations and of the normal stress σ_{yy} at an indentation depth u=40 nm (a and b), at maximum indentation depth (c and d) and after indenter retraction (e and f) for the bare (a, c and e) and coated (b, d and f) bodies.

density becomes very high, it is difficult for new dislocations to glide and provide the required plastic slip, so that effectively the material hardens. The most striking difference between the bare and coated films is that in the coated film there is, from the beginning on, a broader distribution of dislocations and a larger dislocation density (see also Fig. 5).

This happens because when the crystal is coated, the dislocations cannot leave from the top surface and are blocked at the interface with the coating, where they pile up. When the back-stress associated with these pile-ups reaches the source, it suppresses or delays further nucleation, and other sources on nearby slip planes become active. The reduced plasticity found in the coated layer is thus not due to a smaller dislocation density, but to a shorter mean free path of the dislocations, which can thus not contribute as significantly as in the bare crystal to plastic slip. The difference in strain hardening between the bare and the coated layer is more pronounced at very small contact fractions, when the dislocation density is still low, and dislocations in the bare layer can easily access the free surface. At larger contact fractions the dislocation density is so high that the difference fades.

When the indenter is retracted, in the coated crystal the dislocation density decreases only by annihilation of dislocations with opposite Burgers vectors, while in the bare crystal the dislocations can also leave

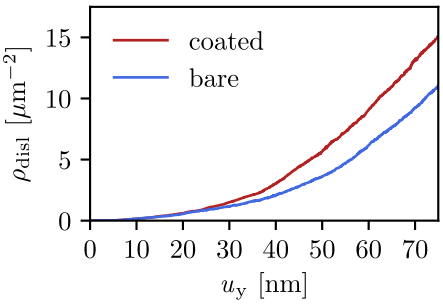

Fig. 5. Dislocations density versus applied displacement for the indentation of a bare and coated crystal to a depth $u = 75$ nm.

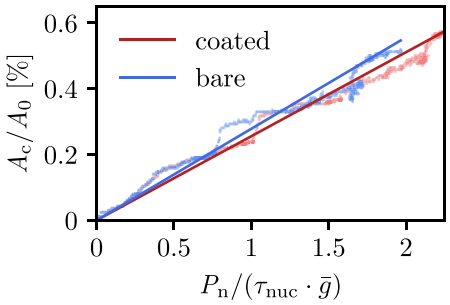

Fig. 6. Contact area fraction versus reduced pressure for the bare (*blue*) and coated (*red*) crystal. (For interpretation of the references to color in this figure legend, the reader is referred to the web version of this article.)

from the top surface. Notice that also in the bare crystal various dislocations do not exit the material, owing to the presence of dislocation obstacles and to entanglements between dislocations on different slip planes. Upon unloading, nucleation of new dislocations continues in both cases, due to the high local stresses generated by the presence of other dislocations close to the nucleation sources.

Note that in Fig. 3(b) we observe a larger contact area for the coated crystal, which is the crystal displaying less plasticity. This might seem in contradiction with the findings by Molinari and coworkers (Pei et al., 2005) where plastic contacts are found to have a larger contact area than elastic contacts. This is not the case, because the contact area in Fig. 3(b) is calculated as a function of indentation depth, which is the input of these simulations. If one presents area as a function of normalized load as in Fig. 6 it is possible to see that, on average, the bare crystal displays a slightly larger contact area at a given pressure.

3.2. Surface roughening

During indentation, the initially flat surface of the two crystals deforms as a consequence of the contact with the rough rigid indenter, which digs some valleys on the flat surface, partly compensated by hills in the surface out-of-contact. The deformed surface profiles of the bare and coated flat crystals are presented at the maximum indentation depth, $u_{\mathrm{y}} = 75$ nm in Fig. 7(a), and after retraction of the indenter in Fig. 7(b). At maximum indentation depth, the differences between the surface profiles of the two crystals are very small. After retraction of the indenter, owing to plasticity, only part of the imposed deformation is recovered. The topography of the two surfaces after retraction becomes significantly different and it is apparent that the surface of the bare crystal presents a finer roughness than the coated one. This additional roughness is caused by the dislocations that have left crystallographic steps of various size while gliding out of the free surface. These steps are also responsible for local differences in the contact area as they form earlier contact with the indenter. Therefore, the resulting contact area of the bare crystal is made of smaller patches, than those in the coated crystal. This can be seen in Fig. 8, where a detail of the deformed surfaces is presented, together with the corresponding contact pressure distribution. The coated surface forms only a single contact area with the indenter, while there are two separate and smaller contact areas in the bare surface. The smaller contact areas formed by the bare surface have to sustain all the contact pressure and thus are characterized by two high peaks in pressure. The pressure profile on the coated surface is much lower and broader.

While the roughening seems rather pronounced on a flat surface, one might wonder whether such roughening would be significant on an already rough surface, that contains very small wavelength. To estimate this, we study the flattening of a rough surface (see Fig. 9) by adopting the assumption typically used in the solution of linear elastic contact problems: the indentation of a flat surface by a rigid rough body corresponds to that of a deformable body with rough surface indented by a rigid flat surface. The validity of this mapping has been demonstrated also in the framework of small strain dislocation plasticity by Ng Wei Siang and Nicola (2016). Following this assumption, the deformed surface of the rough crystal can be obtained at each increment of the simulation by subtracting the height profile of the rough punch from that of the flat surface:

$$y(x) = y_{\mathrm{flat}}(x) - y_{\mathrm{rough}}(x). \tag{2}$$

The flattened surfaces are shown at maximum indentation depth in Fig. 10(a) and after retraction of the flat indenter in Fig. 10(b). Again, the deformed surfaces at maximum flattening do not differ much, and more difference is visible only after retraction of the indenter, given that the coated crystal shows more elastic recovery than the bare crystal. However, differently from the case where the indentation was done on a flat surface, both surfaces appear similarly rough before and after retraction of the indenter. It is not possible to clearly distinguish on the bare surface the additional roughness induced by the dislocations, because the differences are shorter than the smallest wavelengths of the roughness present initially. The dislocations, when leaving the surface from the same slip plane, create surface steps ranging from 0.2 nm to 20 nm. These small differences are responsible of the little changes in local contact area between coated and bare bodies, similar to those described in the previous section, but they have marginal effects on the surface profile, whose smallest wavelength is 20 nm.

The power spectrum of the two rough surfaces after complete retraction of the flat indenter are shown in Fig. 11, and contrasted with the power spectrum of the original surface. The PSD of the three surfaces are indistinguishable in the range of wavelengths of the original surface, as the deformation is rather small and affects only a small region of the surface. It is interesting to see that the roughness of bare and coated layers both extend to smaller wavelengths than the original surface. While the PSD of the bare surface continues at small wavelength approximately on the same line as that of the initial surface, by that almost recovering a self-affine roughness to very small wavelength, the power of the coated surface has a neat drop at the small wavelength of the original surface. This might be an indication that the small roughness is not only caused by dislocations exiting the surface but maybe also, to a much smaller extent, by dislocations that are piling up at the interface. Unfortunately, at small wavelength the power spectrum is very noisy, so it is difficult to extract a clear picture there. Therefore, to further quantify the differences between the deformed surfaces we have computed the root-mean square height, slope and curvature, which are listed in Table 1. Changes in the root-mean-square height are known to be affected mostly by a change in the larger wavelengths, while the slope and even more the curvature are related to the small wavelengths. The deformed coated surface has a root-mean square height that clearly differs from that of the initial surface, due to plastic deformation, while the bare surface has a similar h_{rms}. The presence of the coating has therefore influenced the longer wavelength caused by the deformation. On the contrary, slope and curvature of the coated surface are very similar to those of the original surface, while the values differ significantly between coated and bare.

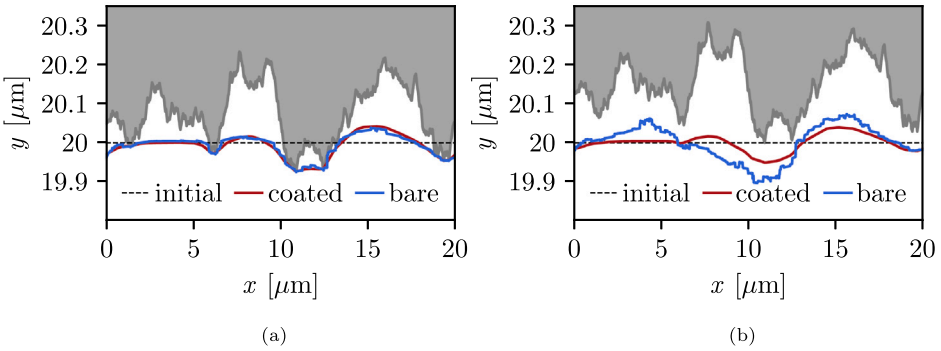

Fig. 7. Height profile of the deformed crystal surfaces at the maximum indentation (a) and after retraction of the indenter (b). The displacement has been magnified in vertical direction for better visualization.

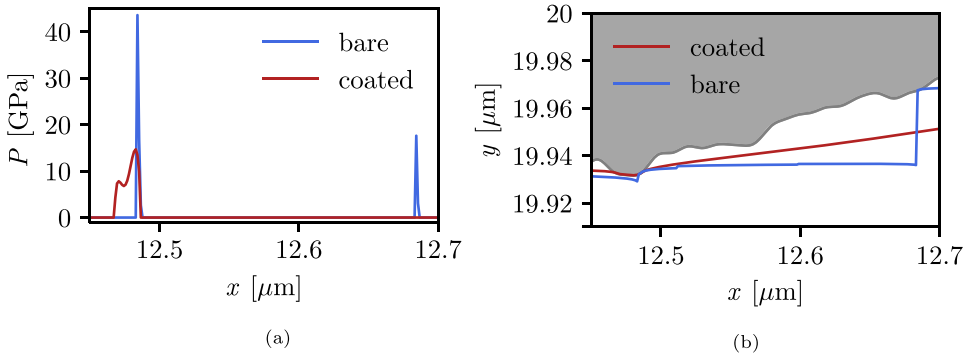

Fig. 8. Nominal and mean contact pressure at an asperity tip (a) and corresponding surface topography (b) (magnified by a factor 100 in the vertical direction) for bare (*blue*) and coated (*red*) metal crystals. (For interpretation of the references to color in this figure legend, the reader is referred to the web version of this article.)

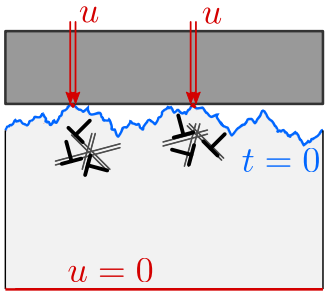

Fig. 9. Schematic representation of the crystal with rough surface in contact with a flat indenter. The crystal is not to scale, it is stretched in vertical direction to visualize the roughness. The symbol ⊤ represents the dislocations.

Table 1
Root-mean-square height (h_{rms}), slope (h_{rms})' and curvature (h_{rms})" for the initial and coated and bare final surfaces.

Surface	h_{rms} [μm]	$(h_{\text{rms}})'$ [ ]	$(h_{\text{rms}})''$ [μm^{-1}]
initial	0.0750	0.3323	23.2866
coated	0.0640	0.3301	23.8822
bare	0.0739	0.6808	498.5477

4. Conclusions

Dislocation dynamics simulations are performed to evaluate the effect of surface roughening during contact loading. To this end, the behavior of bare and coated crystals is contrasted. Results show that when the initial surface is flat, indentation with a rough indenter causes roughening of both crystals. The presence of the coating induces additional strain hardening by preventing the exit of the dislocations, and reducing their mean free path, while their density increases more than in the bare crystal. Upon retraction of the indenter the coated crystal undergoes a more pronounced elastic recovery, and the final deformed surface is smoother than the one of the bare crystal.

The analysis of the power spectral density of the surfaces has shown that the presence of a coating has no impact on the long wavelength in the roughness. This is confirmed by the negligible difference that was found in the root-mean-square height of the deformed surfaces with and without the passivation layer. The coating has instead a significant influence on the very small wavelength, as demonstrated by the differences found between the root-mean-square slopes and curvature of the deformed surfaces. Given that the root-mean-square slope of a surface is known to affect contact area and friction, and considering that both slope and curvature affect adhesion, the presence of a coating, even if its properties are not so different from those of the metal can be beneficial in small-scale applications where friction and adhesion are deleterious, just because it impedes dislocations from gliding out of the body. At larger deformations than the ones considered in this study a different morphology might also have an effect in applications where the gap between surfaces needs to be controlled, to avoid, for instance, leakage of fluids. Apart from the final difference in terms of morphology, also the contact area formation and pressure distribution is affected by dislocations gliding out of the crystal, effects that can also become more relevant at larger deformation. Notice, however, that the differences in morphology in this study affects only wavelength of about 20 nm or smaller. The effect of dislocations gliding out of the surfaces is found to be negligible in crystals that are already rough, considering that the additional roughness provided by the crystallographic steps left by the dislocations are in the order of the small wavelength contained in the roughness of a metal surface.

To highlight the effect of the impenetrable interface and reach an understanding of the effect of exiting dislocations, we have here

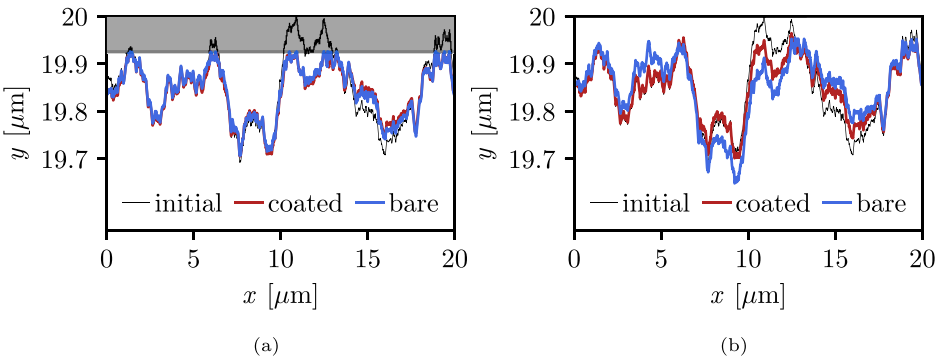

Fig. 10. Height profile of the deformed crystal surfaces at the maximum indentation (a) and after retraction of the indenter (b). The displacement has been magnified in vertical direction for better visualization.

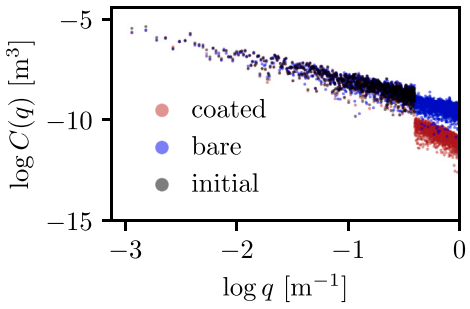

Fig. 11. Power spectrum of the bare and coated layers after retraction of the indenter, contrasted with the PSD of the initial surface.

decided to contrast the same single realization, with and without coating, instead of considering averages over many simulations, as this allows a direct comparison of surface deformation, pressures, internal fields and dislocation distributions. This means also that the results presented in this manuscript are specific of the selected realization. A different realization, either in terms of a different roughness and/or a different spatial distribution of dislocation obstacles and sources will lead to different fields and roughness. We do not expect that the general conclusions will be different, although certainty can only be gained with a statistical representative analysis of various realizations, which is outside the scope of this work.

CRediT authorship contribution statement

R. Civiero: Conceptualization, Software, Data analysis, Data curation, Investigation, Writing – original draft. **F. Perez-Rafols:** Data analysis, Data curation, Supervision. **L. Nicola:** Conceptualization, Supervision, Writing – review & editing, Funding acquisition.

Declaration of competing interest

The authors declare no competing interests.

Data availability

Data will be made available on request.

Acknowledgments

This project has received funding from the European Research Council (ERC) under the European Union's Horizon 2020 research and innovation programme (grant agreement no. 681813).

References

Afferrante, L., Carbone, G., Demelio, G., 2012. Inclusion of 'interaction' in the Greenwood and Williamson contact theory. Wear 278-279, 28–33.
Almqvist, A., Sahlin, F., Larsson, R., Glavatskih, S., 2007. On the dry elasto-plastic contact of nominally flat surfaces. Tribol. Int. 40 (4), 574–579.
Bouchaud, E., 1997. Scaling properties of cracks. J. Phys. Condens. Matter 9 (21), 4319–4344.
Brinckmann, S., Dehm, G., 2015. Nanotribology in austenite: Plastic plowing and crack formation. Wear 338-339, 436–440.
Campañá, C., Müser, M.H., 2007. Contact mechanics of real vs. randomly rough surfaces: A Green's function molecular dynamics study. Epl 77 (3), 38005.
Carbone, G., Bottiglione, F., 2008. Asperity contact theories: Do they predict linearity between contact area and load? J. Mech. Phys. Solids 56 (8), 2555–2572.
Chang, W.R., Etsion, I., Bogy, D.B., 1987. An elastic-plastic model for the contact of rough surfaces. J. Tribol. 109 (2), 257–263.
Chen, Z., Etsion, I., 2019. The elastic–plastic contact behavior of rough surfaces with hard coatings. Tribol. Int. 134, 435–442.
Ciavarella, M., G. J. A, Paggi, M., 2008. Inclusion of 'interaction' in the Greenwood and Williamson contact theory. Wear 265, 729–734.
Gao, Y.F., Bower, A.F., 2006. Elastic–plastic contact of a rough surface with Weierstrass profile. Proc. R. Soc. A Math. Phys. Eng. Sci. 462 (2065), 319–348.
Greenwood, J.A., Williamson, J.B.P., 1966. Contact of nominally flat surfaces. Proc. R. Soc. Lond. Ser. A Math. Phys. Sci. 295 (1442), 300–319.
Hu, Y., Tonder, K., 1992. Simulation of 3-d random rough surface by 2-d digital filter and fourier analysis. Int. J. Mach. Tools Manuf. 32, 83–90.
Ilincic, S., Vorlaufer, G., Fotiu, P.A., Vernes, A., Franek, F., 2009. Combined finite element-boundary element method modelling of elastic multi-asperity contacts. Proc. Inst. Mech. Eng. J J. Eng. Tribol. 223 (5), 767–776.
Irani, N., Nicola, L., 2019. Modelling surface roughening during plastic deformation of metal crystals under contact shear loading. Mech. Mater. 132 (February), 66–76.
Müser, M.H., Dapp, W.B., Bugnicourt, R., Sainsot, P., Lesaffre, N., Lubrecht, T.A., Persson, B.N., Harris, K., Bennett, A., Schulze, K., Rohde, S., Ifju, P., Sawyer, W.G., Angelini, T., Ashtari Esfahani, H., Kadkhodaei, M., Akbarzadeh, S., Wu, J.J., Vorlaufer, G., Vernes, A., Solhjoo, S., Vakis, A.I., Jackson, R.L., Xu, Y., Streator, J., Rostami, A., Dini, D., Medina, S., Carbone, G., Bottiglione, F., Afferrante, L., Monti, J., Pastewka, L., Robbins, M.O., Greenwood, J.A., 2017. Meeting the contact-mechanics challenge. Tribol. Lett. 65 (4), 118.
Ng Wei Siang, K., Nicola, L., 2016. Discrete dislocation plasticity analysis of contact between deformable bodies of simple geometry. Modelling Simul. Mater. Sci. Eng. 24 (4), 45008.
Paggi, M., Ciavarella, M., 2010. The coefficient of proportionality κ between real contact area and load, with new asperity models. Wear 268 (7–8), 1020–1029.
Pei, L., Hyun, S., Molinari, J.F., Robbins, M.O., 2005. Finite element modeling of elasto-plastic contact between rough surfaces. J. Mech. Phys. Solids 53 (11), 2385–2409.
Persson, B.N., 2001a. Elastoplastic contact between randomly rough surfaces. Phys. Rev. Lett. 87 (11), 116101–1–116101–4.
Persson, B.N., 2001b. Theory of rubber friction and contact mechanics. J. Chem. Phys. 115 (8), 3840–3861.
Plouraboué, F., Boehm, M., 1999. Multi-scale roughness transfer in cold metal rolling. Tribol. Int. 32 (1), 45–57.
Pullen, J., Williamson, J.B.P., Tabor, D., 1972. On the plastic contact of rough surfaces. Proc. R. Soc. Lond. Ser. A Math. Phys. Eng. Sci. 327 (1569), 159–173.
Rice, J., 1987. Tensile crack tip fields in elastic-ideally plastic crystals. Mech. Mater. 6, 317–355.
Tiwari, A., Almqvist, A., Persson, B.N., 2020. Plastic deformation of rough metallic surfaces. Tribol. Lett. 68 (4), 129, arXiv:2006.11084.
Van der Giessen, E., Needleman, A., 1995. Discrete dislocation plasticity: A simple planar model. Modelling Simul. Mater. Sci. Eng. 3 (5), 689–735.

Venugopalan, S.P., Nicola, L., 2019. Indentation of a plastically deforming metal crystal with a self-affine rigid surface: A dislocation dynamics study. Acta Mater. 165, 709–721.
Venugopalan, S.P., Nicola, L., Müser, M.H., 2017. Green's function molecular dynamics: Including finite heights, shear, and body fields. Modelling Simul. Mater. Sci. Eng. 25 (3), 34001.
Woo, K.L., Thomas, T.R., 1980. Contact of rough surfaces: A review of experimental work. Wear 58 (2), 331–340.
Xia, W., Dehm, G., Brinckmann, S., 2020. Investigation of single asperity wear at the microscale in an austenitic steel. Wear 452-453, 203289.
Yamada, K., Takeda, N., Kagami, J., Naoi, T., 1978. Mechanisms of elastic contact and friction between rough surfaces. Wear 48 (1), 15–34.